August 27-31, 2023
FLORENCE - ITALY
ICWE 16
16th International Conference on Wind Engineering

Decoupling Wind–Wave–Wake Interactions in a Fixed-Bottom Offshore Wind Turbine

Ondřej Ferčák[1], Juliaan Bossuyt[1], Naseem Ali[2], Raúl Bayoán Cal[1]

[1]*Department of Mechanical and Materials Engineering, Portland State University, Portland, OR, USA, ofercak@pdx.edu*

[1]*Department of Mechanical and Materials Engineering, Portland State University, Portland, OR, USA, jbossuyt@pdx.edu*

[2]*Max Planck Institute for Dynamics and Self-Organization, Göttingen, Germany, naseem.ali@ds.mpg.de*

[1]*Department of Mechanical and Materials Engineering, Portland State University, Portland, OR, USA, rcal@pdx.edu*

SUMMARY:
The interest and benefits of offshore wind energy has also brought along legitimate challenges. In the golden age of renewables, offshore wind-energy holds the most potential for growth, but the burgeoning benefits of offshore energy are also entangled in dynamics not fully understood, such as the dynamic coupling of the atmospheric boundary layer, the wind-turbine generated wake, and the surface waves. This study establishes the first experimental turbulent-interaction between the traditionally distinct fields of airflow-dynamics above the air-sea interface and the characterization of wind-turbine wakes. The study details a non-trivial experimental setup combining a wave tank, wind tunnel, and scaled fixed-bottom wind turbine. Particle image velocimetry (PIV) was performed on three successive image planes to visualize wind-wake, wind-wave, and wave-wake interaction far downstream of the turbine. The wave phase-dependent dynamics of the turbine wake on the passing ocean-wave profile and location are outlined.

Keywords: Turbulence, Particle image velocimetry, Offshore wind energy

1. INTRODUCTION

Public demand for renewable energy, along with advances in research and technology, has driven an exponential increase in wind-energy contribution to the global energy supply over the last two decades (IEA, 2020; "Monthly Energy Review and Electric Power Monthly" February 2021; Snyder and Kaiser, 2009). Offshore wind power is of particular interest due to several benefits: less turbine visibility, higher available wind speeds, and larger turbines, which means increased energy-output potential. However, offshore wind energy is largely underutilized in part because the dynamic influence of the ocean waves on the turbine, its wake, and power production are not well understood.

The loss of momentum within a turbine wake has a negative impact on power production for the downstream rows of turbines and the turbulent interactions between parallel wakes can cause further momentum loss. This momentum deficit accumulates at each row and continues to reduce

the total power density for the farm until a balance is reached between downwards transfer of mean kinetic energy and power extracted by the turbines (Bossuyt et al., 2018; Cal et al., 2010).

What is unclear in the case of offshore wind farms, is how ocean waves affect a turbine's wake profile and whether they have a positive or negative effect on its wake recovery. These ocean wave-wake interactions also have implications on the net forces felt by the turbine tower and rotor (Medici and Alfredsson, 2006; Van Binh et al., 2008), and can even influence meteorological effects (Baidya Roy et al., 2004). This means that characterizing the interaction between the ocean waves and wake, and the resulting turbulent stresses, is needed to fully understand offshore wake dynamics used for design and optimization.

This study details a novel experimental setup combining a wave tank, wind tunnel, and scaled fixed-bottom wind turbine, and provides the first experimental measurement for offshore wind turbine wave-wake interactions. A fixed turbine was selected to isolate the three main variables (wind, wake, and wave) from the additional frequency dynamics of a floating turbine. A particle image velocimetry (PIV) set-up was modified to include a water wave-tank and wave generator, to simulate long-period deep-water ocean waves. Three successive image-planes were captured to visualize the wind-wake, wind-wave, and wave-wake interactions far downstream of the turbine. The instantaneous PIV snapshots were synchronized and decomposed according to the respective wave phases, to identify and quantify phase-dependent modulation of the wind-turbine wake by the ocean wave.

2. EXPERIMENTAL SETUP

The experiments of a scaled fixed bottom wind turbine were performed in the closed-loop wind and water tunnel at Portland State University. For this purpose, the wind tunnel floor was replaced with a customized water-tank to simulate deep ocean wave conditions. The wind tunnel test section had a height of 0.8 m, width of 1.2 m and test-length of 5 m. Based on the wind tunnel size, a diameter of 0.15 m was selected for the scaled wind turbine, resulting in a geometric scaling ratio of 1:600 in comparison to a full scale turbine with a diameter of 90 m. The water tank covered the full wind tunnel floor and provided a water depth of 0.3 m, corresponding to a water depth of 180 m in full-scale. The tank was isolated from the wind tunnel to reduce vibration and was supported with anti-vibration leveling feet. The wind-tunnel side-walls were assembled of schlieren-grade annealed float glass fastened to the aluminum framework to ensure maximum access for the laser and camera. The wind tunnel speed had a range between 2 and 40 ms^{-1}. The tunnel ceiling was configured to approach a zero-pressure gradient boundary layer. A wave paddle was positioned at the entrance of the test-section, and was controlled by a stepper motor to produce scaled long-period deep-water waves. At the end of the test-section a custom made static wave damper was used to absorb the incoming waves.

Particle image velocimetry was used to measure 2D-2C velocity fields in streamwise aligned planes. The PIV setup consisted of a 4 megapixel CCD camera and a Litron Nano double pulsed Nd:YAG (532 nm, 1200 mJ, 4 ns duration) laser. The camera lens had a focal length of 50 mm. Neutrally buoyant fluid particles of diethyl-hexyl sebacate were aerosolized by a seeding generator with a constant density throughout the experiment. For each measurement 3000 independent

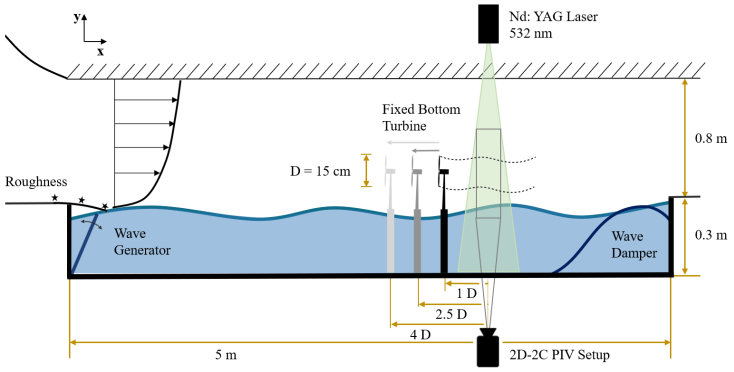

Figure 1. Schematic representation of the experimental setup. Image not to scale.

image-pairs were recorded at a frequency of 4 Hz. DAVIS 8.4 software was used to apply a multi-pass Fast Fourier Transform (FFT) based cross-correlation algorithm and a universal outlier detection method to filter out unwanted vectors from the PIV data. A multiple-pass reducing size interrogation window of 64 $\times$ 64 pixels and 32 $\times$ 32 pixels, with a 50% overlap was used to process the data. The PIV window covers an area of 0.2 m$\times$ 0.2 m.

3. RESULTS

The inflow is advected from left to right and the turbine origin is located at x/D = 0. Time averaged $\overline{u}$ and phase-averaged $\overline{u}_\phi$ streamwise mean velocities are presented in Figure 2 for two wave-frequencies. Figures 2(a) and 2(b) show the ensemble-averaged streamwise velocity profiles ($\overline{u}/\overline{u}_\infty$) for wave frequencies of 2 Hz and 1.25 Hz, respectively. The classic wake profile shows a region of reduced momentum directly behind the turbine hub, which slowly recovers downstream. The standard deviation (s_i) of the wake-center is approximately linear and ranges from a mean of y/D = 0.04 at x/D = 1 and y/D = 0.17 at x/D = 5. As the wake moves downstream, the wake center drifts down toward the water line. This effect is present for both wave frequencies but is slightly more pronounced for the longer wave-length in Figure 2(b). This effect is known to be due to the shear stress ($\overline{u'v'}$) in the mean velocity, and is counteracted by the shorter wave length in Figure 2(a) through increased wave-frequency, increased wave-height, or both. Both phenomena are discussed in more detail in the following sections. High velocity regions can also be seen near the wave and turbine (lower-left) in both figures. However, in Figure 2(a), this region extends a shorter lateral distance and is lower in magnitude than is seen in Figure 2(b). This disparity is likely due to the larger disruption of the inflow from high frequency (2 Hz) waves in Figure 2(a) versus the long wave length (1.25 Hz) in Figure 2. It is worth noting that the low frequency (1.25 Hz) wave has a greater wave speed, at c = 1.2 m/s, compared to the high-frequency (2 Hz) wave at c = 0.7 m/s. The free-stream velocity (5.9 m/s) was significantly greater than either wave speed. However, to illustrate the importance of this point, any normalized velocity $u/u_\infty < 0.12$ for the shorter wave-length frequency (2 Hz) is moving slower than the wave itself (Fig. 2(a), 2(c), 2(e), 2(g), and 2(i)). For Figures 2(b), 2(d), 2(f), 2(h), and 2(j), any velocity $u/u_\infty < 0.2$ is moving slower than the wave. This implies that, as wave speeds approach that of the free-stream velocity ($c \rightarrow \overline{u}_\infty{}^-$), there is less likelihood that the wave itself can impart momentum into the system, as is the case for $c^*{}_{1.25Hz} = 4.9$, which behaves more like a moving obstruction, as compared to ${c_{1.25Hz}}^* = 4.9$.

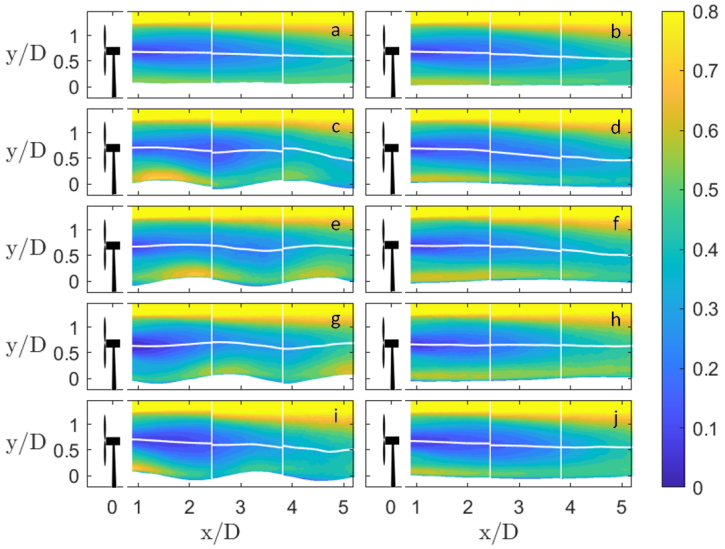

Figure 2. Normalized streamwise velocity profiles for 5.9 m/s inflow. Wake center is shown in white: (a) ensemble-average for 2 Hz wave and (b) ensemble-average for 1.25 Hz wave and (c) phase-average, $\phi = 1$, for 2 Hz wave and (d) phase-average, $\phi = 1$, for 1.25 Hz wave and (e) phase-average, $\phi = 2$, for 2 Hz wave and (f) phase-average, $\phi = 2$, for 1.25 Hz wave and (g) phase-average, $\phi = 3$, for 2 Hz wave and (h) phase-average, $\phi = 3$, for 1.25 Hz wave and (i) phase-average, $\phi = 4$, for 2 Hz wave and (j) phase-average, $\phi = 4$, for 1.25 Hz wave.

4. CONCLUSIONS

This experiment considered a scaled fixed-bottom wind turbine under two wind conditions and three wave conditions inside an augmented wind tunnel, retrofitted with a wave-generating wave tank. PIV measurements were collected at three separate downstream locations to generate the velocity fields directly behind, and far downstream, of the turbine. The PIV snapshots were also used to detect the instantaneous wave profiles and used to sort the velocity fields into like wave-phase averages.

REFERENCES

Baidya Roy, S., Pacala, S. W., and Walko, R., 2004. Can large wind farms affect local meteorology? Journal of Geophysical Research: Atmospheres 109.

Bossuyt, J., Meneveau, C., and Meyers, J., 2018. Effect of layout on asymptotic boundary layer regime in deep wind farms. Physical Review Fluids 3, 124603.

Cal, R. B., Lebrón, J., Castillo, L., Kang, H. S., and Meneveau, C., 2010. Experimental study of the horizontally averaged flow structure in a model wind-turbine array boundary layer. Journal of Renewable and Sustainable Energy 2, 013106.

IEA, P., 2020. World wind electricity production by region. https://www.iea.org/data-and-statistics/charts/world-wind-electricity-production-by-region-2005-2018.

Medici, D. and Alfredsson, P., 2006. Measurements on a wind turbine wake: 3D effects and bluff body vortex shedding. Wind Energy: An International Journal for Progress and Applications in Wind Power Conversion Technology 9, 219–236.

Monthly Energy Review and Electric Power Monthly, February 2021. Boundary-Layer Meteorology.

Snyder, B. and Kaiser, M. J., 2009. A comparison of offshore wind power development in Europe and the US: Patterns and drivers of development. Applied Energy 86, 1845–1856.

Van Binh, L., Ishihara, T., Van Phuc, P., and Fujino, Y., 2008. A peak factor for non-Gaussian response analysis of wind turbine tower. Journal of Wind Engineering and Industrial Aerodynamics 96, 2217–2227.